CrossMark

The Oxide-Scale Growth and Failure on an Fe–16Cr Alloy in the Presence of Compressive Stress

C. H. Zhou[1] · A. L. Liu[1] · H. T. Ma[2] · L. Wang[2]

Abstract The high temperature oxidation behavior of an Fe–16Cr binary alloy, oxidized under different compressive stresses in air at 900 °C, was investigated. Surface and cross-sectional micrographs, observed by scanning electron microscopy, indicated that the resulting morphology of the thermally grown oxide scale depended on the compressive stress. Results showed that oxide scales were infact below 5 MPa stress after 10 h of oxidation. Delamination developed at the outer/inner oxide scale interface in the case of compressive stress above 5 MPa. Growth kinetics measurements revealed that the rate of oxide-scale growth increased by the compressive stress.

Keywords High temperature oxidation · Compressive stress · Kinetics · Failure · Fe–Cr alloy

Introduction

The formation of an oxide scale on an alloy could serve to provide protection against further attack. However, in most practical applications protective oxide scales are subjected to stresses, either by mechanical loading or by the oxidation process itself. Therefore, oxide scales are prone to damage in several manners [1]. Compared with a stress by the oxidation process itself, the effect of mechanical loading on the high-temperature oxidation behavior of alloys is more significant. More and more investigations have been conducted to explore the affect of

✉ C. H. Zhou
dlut2325@163.com

1   School of Material Science and Engineering, Heilongjiang University of Science and Technology, Harbin 150022, China

2   School of Material Science and Engineering, Dalian University of Technology, Dalian 116085, China

mechanical loading on the oxidation of alloys. Extensive studies have confirmed the fact that the application of tensile loading to a material increases the oxidation rate [2–4]. There is also some published information on the effect of external stresses on the oxide-scale integrity, adhesion, cohesion and cavities developed at the oxide/metal interface [5–8]. All of these studies indicate that the growth and protectiveness of oxide scales are severely affected by mechanical loading. However, there are still many unclear phenomenon to be explored [5].

Iron-chromium steels have been widely used in process industry and power plants owing to their excellent oxidation resistance at high temperatures. The effect of a imposed tensile loading on the oxidation behavior of Fe–Cr binary alloys has been studied [9, 10]. It was anticipated, based on the fact that the scales should be elongated and hence prone to cracking, that the oxidation rate could be accelerated by the tensile loading. However, no accelerated oxidation was observed for ferritic alloys (Fe–20 %Cr and Fe–18 %Cr). The absence of acceleration was suggested to be attributed to the rapid healing of oxide scale by virtue of the relatively high diffusion rate of Cr in the alloys. If the Cr concentration in Fe–Cr alloys is lowered to a critical value, healing of the oxide scale would not occur. Then, a different effect of mechanical loading on oxidation behavior may be observed. Moreover, the oxide-scale growth and failure under a compressive stress are actually different from that under a tensile stress [11–13]. Therefore, the present study attempted to explore and assess the oxidation behavior of an Fe–16Cr alloy in the presence of compressive stresses.

Materials and Experimental Procedures

The alloy with nominal composition of Fe–16Cr alloy was used. The actual composition determined by an energy dispersive spectrometer (EDS) was Fe–15.69Cr (in wt%). Samples with dimensions of $8 \times 8 \times 12$ mm and $2 \times 8 \times 12$ mm were cut from plates for compressive test and for comparing test without stress, respectively. All samples were mechanically ground on successively finer abrasive SiC papers down to a 2000 grit finish (2.5 μm). Prior to oxidation, the samples were cleaned with acetone and then ethanol. After drying, the samples were subjected to the oxidation tests.

The compressive oxidation test was carried out by the universal testing machines using the high temperature components. Figure 1 shows the schematic diagram of oxidation apparatus and the tested oxide-scale position. During the compressive test, the sample was placed into the furnace when the temperature reached to 900 °C, but it dropped temporarily to 850 °C approximately before increasing to 900 °C in about 2 min. The compressive stress was applied when the sample was placed into the furnace. When the temperature was 900 °C again, the oxidation time was recorded. At the end of the test, the sample was removed from the furnace and cooled down to room temperature in air. After each test, compositions and surface, cross-sectional morphologies of oxide scales were examined by using scanning electron microscopy (SEM) equipped with EDS and electron probe microanalysis (EPMA).

The oxidation kinetics was carried out by measuring the oxide-scale thickness which Fe–16Cr alloy oxidized at different conditions. Firstly, a series of oxidation
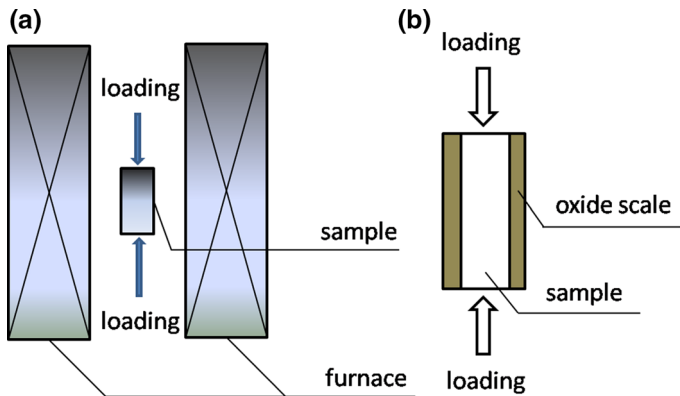
Fig. 1 Schematic diagram of oxidation apparatus (**a**) and the tested oxide-scale position; (**b**) directions of the applied loading and the growth of oxide scale

experiments at several intervals were performed. Then the related cross-sectioned morphologies were observed by SEM. After that, the average oxide-scale thickness was measured by using Q500IW image analysis meter. Finally, the relations between average oxide-scale thickness and corresponding oxidized time were plotted as a fully kinetics curve. During the measurement of oxide-scale thickness, at least 5 SEM images were used. And the mean oxide-scale thickness was measured by different SEM images. It is noted that the measured thickness was not consisted of the separated gaps generated in oxide scales.

Results

Observation of Surface and Cross-Sectional Morphologies

Figure 2 shows the surface morphologies for Fe–16Cr alloy oxidized under compressive stresses at 900 °C for 10 h. As indicated in Fig. 2a–c, the oxide scale appeared to spall when the compressive stress exceeded 5 MPa. Up to 10 MPa, only several local external oxide scales were left, as shown in Fig. 2c. The semi-quantitative analysis on the relation between spalled area and compressive stress in Fig. 2d implies the oxide scales abrupt spall after exceeding 5 MPa stress. The high magnification surface morphological images in Fig. 2e, f indicate that the oxide scales are comprised of cone-shaped base and net structure around them, which is accordance with the previous investigations [9, 10].

A special cross-section of Fe–16Cr alloy oxidized under 5 MPa at 900 °C for 10 h is shown in Fig. 3. It can be seen that the oxide scales are consisted of two distinguishable zones marked out by dotted line, i.e., outer oxide layer and inner oxide layer. Out oxide layer shows outward buckling multi-layer morphologies. Though the oxide scales was quite integrity in Fig. 2a, obvious delamination existed in the outer oxide scale and at the outer/inner oxide scale interface.
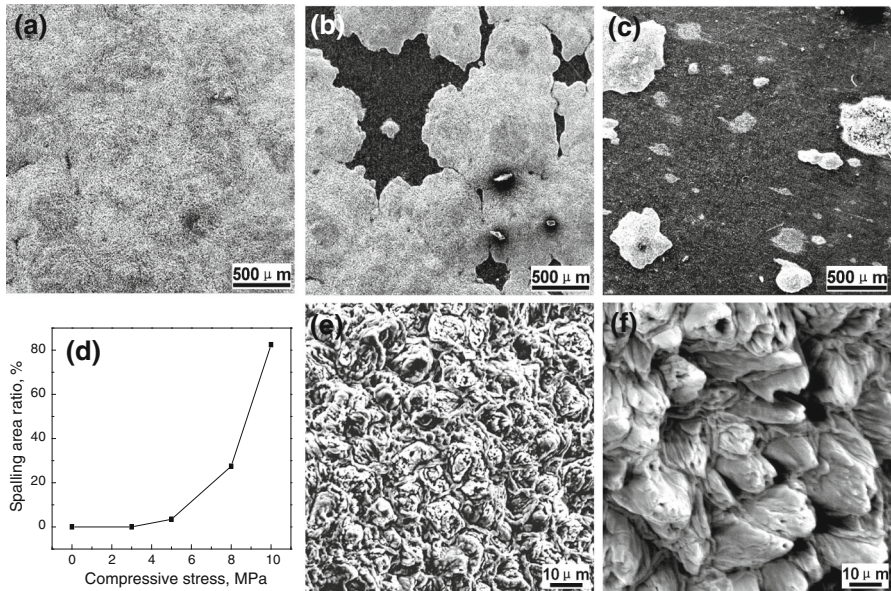
Fig. 2 Surface morphologies for Fe–16Cr alloys oxidized under compressive stress at 900 °C for 10 h. **a** 5 MPa; **b** 8 MPa; **c** 10 MPa; **d** the relation between spallation area and compressive stress; **e** high magnification surface image, 5 MPa; **f** high magnification surface image of un-spalled zone, 10 MPa

Fig. 3 Cross-sectional morphologies for Fe–16Cr alloys oxidized under 5 MPa compressive stress at 900 °C for 10 h
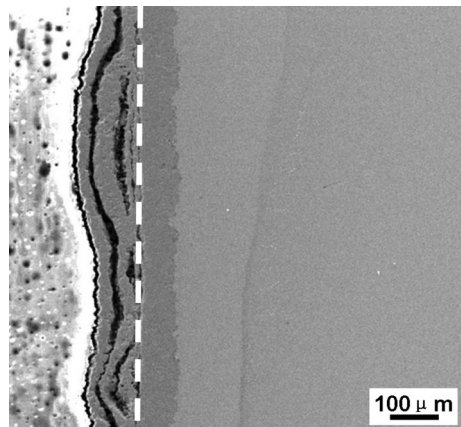
Oxide-Scale Growth

The relation between oxide-scale thickness and time is shown in Fig. 4. It can be noticed that the oxide-scale growth increases with the increasing stress below 5 MPa. At 8 MPa stress, the oxide-scale growth is similar with that of 5 MPa. The corresponding parabolic plots are given in Fig. 5. It can be seen that the growth of Fe–16Cr alloy oxidized under compressive stress follows a parabolic law. After
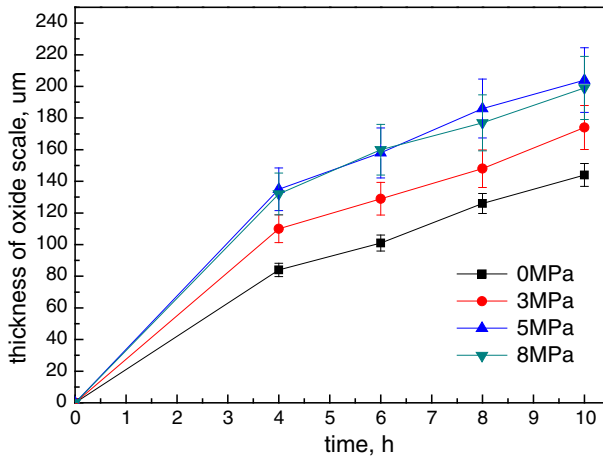
Fig. 4 The thickness of oxide scale as a function of time for Fe–16Cr alloy oxidized under compressive stress in air at 900 °C. (Note: The thickness of oxide scale at 8 MPa was measured at the un-spalled zone.)
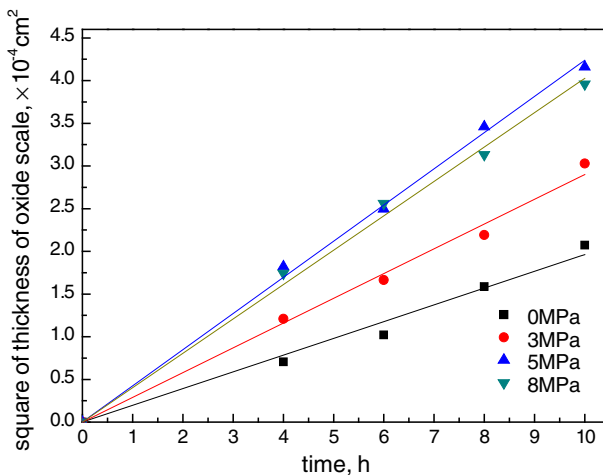

Fig. 5 The square of thickness of oxide scale as a function of time for Fe–16Cr alloy oxidized under compressive stress in air at 900 °C

calculating, the oxidation rate constant for unstressed condition is equal to $5.5 \times 10^{-9} \text{cm}^2/\text{s}$. At 3 MPa stress, the oxidation rate constant is equal to $8.1 \times 10^{-9} \text{cm}^2/\text{s}$, which is somewhat higher than that of unstressed condition. At 5 MPa stress, the oxidation rate constant is equal to $1.2 \times 10^{-8} \text{cm}^2/\text{s}$, which exceed the unstressed oxidation rate constant by a factor of 2. At 8 MPa stress, the oxidation rate constant is equal to $1.1 \times 10^{-8} \text{cm}^2/\text{s}$, which is similar with that at 5 MPa stress. Those oxidation rate constants under compressive stress are close to the oxidation rate constant ($5.3 \times 10^{-8} \text{cm}^2/\text{s}$) of pure Fe at the same temperature

calculated by the data in literature [14]. The fact verifies that the applied compressive stress significantly increased the oxide-scale growth of Fe–16Cr alloy.

Discussion

Oxide-Scale Growth

Figure 6 and Table 1 show EPMA chemical element mapping of Fe–16Cr alloy oxidized under 5 MPa stress for 10 h. It can be seen that the oxide scales comprise two obvious oxide layers of an outer iron-oxide layer and an inner mixture of iron- and chromium-oxide layer. EPMA chemical element mapping shows that the Fe/O
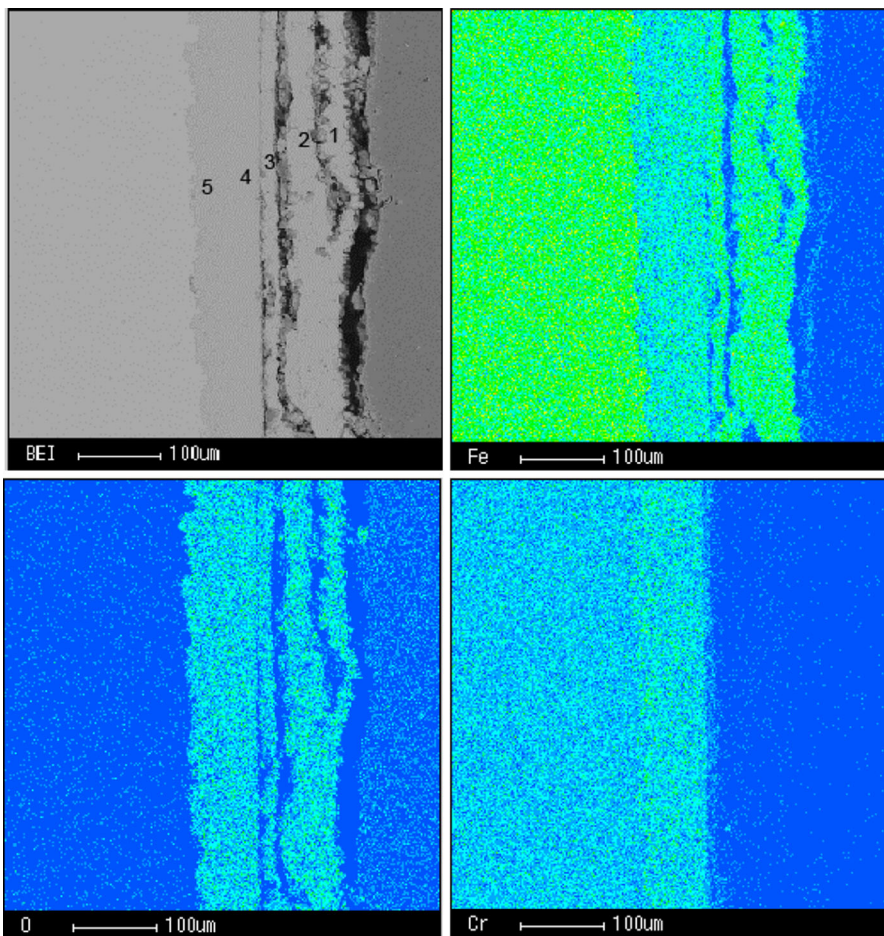

Fig. 6 Cross-sectional BEI micrograph of Fe–16Cr alloys oxidized at 900 °C in air for 10 h and X-ray maps of Fe, O, Cr under the stress of 5 MPa

Table 1 Quantitative analysis results of the scales formed on the Fe–16Cr alloys during oxidation subjected to a stress of 5 MPa for 10 h as shown in Fig. 6

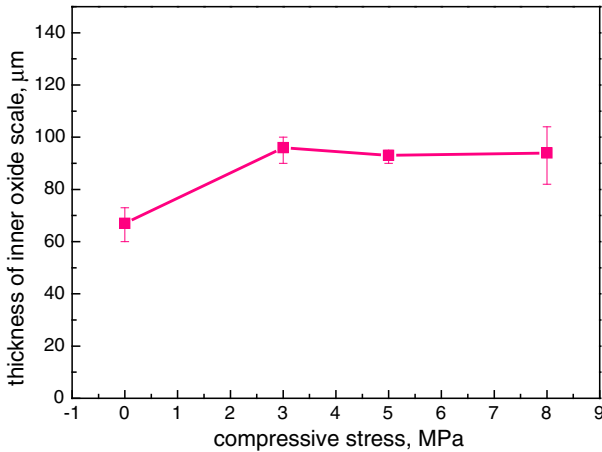| Location	Composition (at%)		
	Fe	Cr	O
1	39.91	–	60.09
2	43.38	–	56.62
3	47.58	–	52.42
4	33.04	15.67	51.29
5	37.76	15.78	46.46

Fig. 7 The thickness of inner oxide scale as a function of compressive stress for Fe–16Cr alloy oxidized under compressive stress in air at 900 °C for 10 h

radio of point 1 is about equal to 2:3, which is implied to be an outmost Fe_2O_3 oxide layer. The Fe/O radio of points 2, 3 is somewhat smaller than 1, but bigger than 2:3. It may be the mixtures of Fe_3O_4 and FeO. The points 4, 5 contain Cr element, which is different with point 1, 2, 3. The (Fe + Cr)/O radio is approximately equal to 1, which is mostly the mixed spinel $Fe(FeCr_2)O_4$ according to the Fe–Cr–O phase [14]. Those are accordance with the previous investigation on the oxidation behavior of Fe–Cr alloys [9, 10, 14–21].

The growth of inner oxide scales under compressive stress was investigated. The corresponding kinetics curves in the form of analyzing the relation between thickness of inner oxide scale and compressive stress are shown in Fig. 7. It can be seen that the applied stresses contribute to a somewhat increase in the thickness of the inner oxide scale, but there was no obvious change for different stress level, i.e., the thicknesses of inner oxide scale formed under the stress from 3 to 8 MPa are similar.

According to the growth kinetics in Figs. 4, 5, and 7 and EPMA chemical element mapping in Table 1, it can be ensured that the increased oxide-scale growth is related to the growth of external iron-oxide layer. As the iron-oxide scales are prone to crack and even spall, the short-circuit diffusion maybe the main growth-controlling factor on the increased growth of iron-oxide scales. Those crack formations in the iron-oxide

scales have been detected by many investigations. Ikeda et al. [22] detected such cracks which generated during oxidation of Fe–Cr alloys containing 5–20 %Cr by "sulfur-decoration" method. Christl et al. [23] also found microcracks generated in Fe_3O_4 layer during oxidation of 2.25Cr–1Mo steel. Subjecting a compressive stress to the samples, the oxide scales are more prone to crack owing to the lower ductility of iron-oxides. Then the short-circuit diffusion is enhanced and therefore the growth of Fe-oxide layer is increased. Once the amount of cracks in scales increases to a critical value with the increasing compressive stress, the Fe-oxide layer begins to separate from the internal oxide layer and subsequently to spall.

   Besides the changes of microstructure and chemical composition, the external oxide scales are locally detached from the internal scale and show multilayer characteristics in the case of a 5 MPa stress, as indicated in Figs. 3 and 6. This phenomenon is related to the compressive stress on the buckling feature of oxide scale. The critical buckling strain $\varepsilon_{\mathrm{II}}^{\mathrm{init}}$ is given by [24]:

$$\varepsilon_{\mathrm{II}}^{\mathrm{init}} = \frac{1.22}{1 - v^2} \left(\frac{h}{R}\right)^2 \qquad (1)$$

where v is the Possion's ratio of the oxide scale, h is the thickness of oxide scale, 2R is the diameter of the initial decohesion. Because of the applied compressive stress and the coordinate changes of oxide scale and alloy interface, the oxide scale would undergo higher strain. Then the diameter of the initial decohesion deceases, which results in the oxide scales buckling outside. Therefore, cavities, voids even separation appear at the outer/inner oxide scale interface. This process is different with that under tensile stress/strain. In tensile creep tests, the dislocation climbs reduce the vacancy concentration near scale-metal interface region and drive the vacancies into metal. Gibbs and Hales have proposed the equation for the rate of thickening of an oxide scale with vacancy concentration [25]. Rolls, Stroosnijder et al. have analyzed the effect of tensile stress on the interface reaction by experimental results [2, 4], suggesting cation vacancy annihilation at the external and internal scale interface plays a role in the growth of oxide scale. According to the analysis of tensile stress/strain effect on the growth of oxide scale, the growth of oxide scale in the presence of compressive stress would decrease with the increasing stress. On contrary, however, the whole oxide-layer growth is increased by the applied stress lower than 5 MPa, as shown in Fig. 4. The authors suggested that it should be attributed to the new Fe-oxide formation in the cavities, voids or separation. At 900 °C, the partial pressure $p_{O_2} = 1.8 \times 10^{-17}$ atm for $Fe + 1/2O_2 \rightarrow FeO$ [26], the new FeO would form on the surface of mixture oxide layer in the cavities, voids or separation because Cr has been depleted to form Cr_2O_3 dispersed phase as above analysis. Thus, new oxide layer generate and grow to maintain the continuous oxide-scale growth. Once the new formed Fe-oxide layer was detached from the beneath layer, cavities, voids or separation would be generated between the both layers. Then the new Fe-oxide will form in those cavities, voids and separation again. This process is cycled and multilayer morphology is formed after a long exposure under compressive stress. Figure 8 displays the cross-sectional morphologies of Fe–16Cr alloy oxidized without and with 5 MPa stress for 20 h. It can
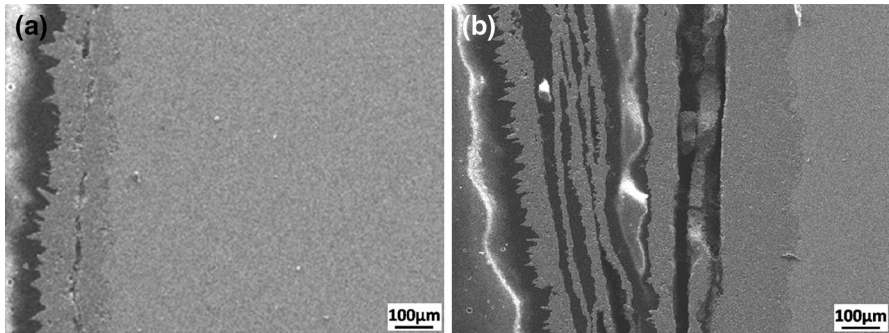
Fig. 8 Cross-sectional morphologies for Fe–16 %Cr alloy oxidizing under compressive stress at 900 °C for 20 h. **a** 0 MPa; **b** 5 MPa

be seen that the oxide scale of the unstressed sample was still closely contacted with the alloy. While the oxide scale of the stressed sample showed the typical multilayer morphology, just like the above analysis. In all, the application of compressive stress induces outer iron-oxide short-circuit diffusion and the formation of cavities at the outer/inter oxide scale interface and within the outer oxide scale, in where new iron-oxide layer forms.

Oxide-Scale Failure

Nagl [8] summarized the mechanical oxide-scale failure under compressive load. Generally, the oxide-scale failure mechanism proposed by Evans is widely used to analyze cracking and spallation of the oxide scales [27, 28]. Seen from the micrographs in Figs. 3, 6, and 8, it can be gained that oxide-scale failure under a compressive stress is mainly external iron-oxide layer failure. Under compressive conditions, the compressive stress induced the outer Fe-oxide layer buckling outside, which results in the cavities forming at the outer/inner oxide scale interface. Then the interface is weakened, and the iron-oxide layer is prone to detach from the inner oxide scale. If the oxidation time is short, the compressive strain is so small that can not lead to the oxide-scale spallation. After exceeding the critical spallation strain [27], ε_{II}^{spall}, the buckled oxide scale would crack and eventually spall, as shown in Fig. 2. In addition, the growth of Fe-oxide makes the oxide scale hardly strain tolerance because of their lower ductility, thus the oxide scales are prone to crack. So, based on the oxide-scale failure mechanism proposed by Evans, the failure mechanism of oxide scales on Fe–15Cr alloy under compressive stress is 'weak interface and strong oxide' model.

Conclusions

Compressive samples of an Fe–16Cr alloy were subjected to oxidation at 900 °C with the stresses in the range of 3 to 10 MPa. The oxide-scale surface and cross-sectional morphologies were examined. The major conclusions from this investigation were:

1. Compressive stress induced an increase in growth of the oxide scales on Fe–16Cr alloy
2. Compressive stress induced delamination of the outer Fe-oxide layer from the inner mixture of iron- and chromium-oxide layer
3. Failure of the oxide scales formed on the samples subjected to a compressive stress was weak interface and strong oxide.

References

1. M. Schütze, *Materials Science and Technology* **4**, 1988 (407).
2. R. Rolls and M. H. Shahhosseini, *Oxidation of Metals* **18**, 1982 (115).
3. G. Calvarin-Amiri, R. Molins and A. M. Huntz, *Oxidation of Metals* **54**, 2000 (399).
4. M. F. Stroosnijder, V. Guttmann, R. J. N. Gommans and J. H. W. de Wit, *Materials Science and Engineering* **121**, 1989 (581).
5. S. R. Pillai, N. S. Barasi and H. S. Khatak, *Oxidation of Metals* **49**, 1998 (509).
6. J. Robertson and M. I. Manning, *Materials Science and Technology* **6**, 1990 (81).
7. H. E. Evans, *Materials Science and Technology* **1988**, 1089 (4).
8. M. M. Nagl and W. T. Evans, *Journal of Materials Science* **28**, 1993 (6247).
9. S. Leistikow, I. Wolf and H. J. Grabke, *Werkstoffe und Korrosion* **38**, 1987 (556).
10. Y. Ikeda and K. Nii, *Journal of Japan Institute of Metals* **47**, 1983 (191).
11. C. H. Zhou, H. T. Ma and L. Wang, *Corrosion Science* **52**, 2010 (210).
12. C. H. Zhou, H. T. Ma and L. Wang, *Oxidation of Metals* **70**, 2008 (287).
13. C. H. Zhou, H. T. Ma and L. Wang, *Materials and Corrosion* **61**, 2010 (676).
14. D. J. Young, *High Temperature Oxidation and Corrosion of Metals*, (Elsevier, The Netherlands, 2008).
15. I. R. Sohn and T. Narata, *Oxidation of Metals* **59**, 2003 (353).
16. T. Amano, A. Hara, N. Sakai and K. Sasaki, *Materials at High Temperatures* **17**, 2000 (117).
17. E. Park, B. Huning, S. Borodin, M. Rohwerder and M. Spiegel, *Materials at High Temperatures* **22**, 2005 (567).
18. C. Ostwald and H. J. Grabke, *Corrosion Science* **46**, 2004 (1113).
19. M. Seo, G. Hultquist, F. Baba and N. Sato, *Oxidation of Metals* **25**, 1986 (163).
20. I. G. Crouch and J. C. Scully, *Oxidation of Metals* **15**, 1981 (101).
21. R. Y. Chen and W. Y. D. Yuen, *Oxidation of Metals* **57**, 2002 (53).
22. Y. Ikeda and K. Nii, *Oxidation of Metals* **12**, 1978 (487).
23. W. Christl, A. Rahmel and M. Schütze, *Oxidation of Metals* **31**, 1989 (1).
24. J. Timoshenko and N. Goodier, *Theory of Elasticity*, 3rd ed, (McGraw-Hill, New York, 1969).
25. G. B.Gibbs and R. Hales, in *Proceeding of the Conference on Vacancies'76*, eds. R. E. Smallman and J. E. Harris (The Metals Society, Bristol, 1977), p. 201.
26. D. J. Young, *High Temperature Oxidation and Corrosion of Metals*, (Elsevier Ltd., Boston, 2008).
27. H. E. Evans and T. C. Lobb, *Corrosion Science* **24**, 1984 (209).
28. H. E. Evans, *International Materials Reviews* **40**, 1995 (1).